J. Comp. App. Res. Mech. Eng. Vol. 13. No. 2, pp. 169-180, 2024 *DOI: 10.22061/JCARME.2023.9030.2221*

SRTTU

Journal of Computational and Applied Research in Mechanical Engineering

jcarme.sru.ac.ir

JCARME

ISSN: 2228-7922

Research paper

Numerical solution of unsteady incompressible nanofluid flow with mixed convection heat transfer using Jameson method on unstructured grid

S. Rasoolzadeh and M. Y. Hashemi*

Department of Mechanical Engineering, Azarbaijan Shahid Madani University, Tabriz, 53751-71379, Iran

Article info:

Article history:

Received: 11/05/2022

Revised: 18/09/2023

Accepted: 20/09/2023

Online: 23/09/2023

Keywords:

Unsteady numerical simulation,

Jameson method,

Cu-water nanofluid,

Artificial compressibility,

Mixed convection heat transfer.

***Corresponding author:**

m.y.hashemi@azaruniv.ac.ir

Abstract

The purpose of this paper is to numerically simulate unsteady, incompressible, and laminar flow with natural and mixed convection heat transfer in a square lid-driven cavity filled with Cu-Water nanofluid. Jameson method is used in conjunction with the Artificial compressibility method on the unstructured grid in a viscous flow. Effects of Grashof number and nanoparticle volume fraction on the flow and heat transfer characteristics are investigated. Two-dimensional Navier-Stokes equations as the governing equations of the problem are discretized with the finite volume method. Spatial discretization is performed with a two-order central scheme; and Jameson artificial dissipation terms are added to equations to stabilize the solution. Unsteady terms are discretized with an implicit two-order scheme and are solved with fourth-order explicit Runge-Kutta method in pseudo-time. It is found that the Jameson method has good performance with a reasonable convergence rate. Results show that an increase in the volume fraction of nanoparticles improves heat transfer characteristics while the increase in the Grashof number, weakens the heat transfer due to the domination of natural convection.

1. Introduction

Numerical solutions of incompressible Navier-Stokes equations as the governing equations of incompressible fluid flows are widely investigated in literature due to their extensive applications in industry such as heat exchangers and cooling systems in electronic devices and nuclear reactors. Lack of a relation between continuity and momentum equations is the main issue in this system of equations. The artificial compressibility (AC) method, which was introduced by Chorin, is an efficient way to overcome this issue. AC method was originally formulated by Chorin [1] for steady incompressible flows, but it was very soon extended to unsteady flows for both laminar and turbulence regimes. Malan *et al.* [2] developed a

robust AC scheme to model laminar steady state and transient incompressible flows. They used this scheme to solve several laminar examples and declared that this method is easy to use and has enough accuracy over a wide range of Reynolds and Rayleigh numbers [3]. Louda *et al.* [4] investigated a comprehensive study on the solution of steady unsteady laminar and turbulent flows by AC method. They examined both single-time and dual-time stepping approaches as the extension for unsteady simulation. They concluded that in the single-time method, the magnitude of the artificial compressibility coefficient (β) is bounded due to computational reasons; and the results of the single-time method for unsteady flows are not reliable but the dual-time approach works well for laminar and turbulence unsteady flows. Also, Liang *et al.* [5] used the dual-time stepping AC method to solve incompressible Taylor-Couette flow and a laminar flow over an oscillating cylinder.

Due to its efficient performance, ACM has been coupled with other methods so that a more accurate scheme with a higher convergence rate can be obtained. Tang and Sotiropoulos [6] combined the pressure-based and fractional step formulation with the standard AC method. They solved different 2D and 3D problems and showed that the hybrid fractional-step/artificial-compressibility (FSAC) method requires considerably less CPU time in comparison with the original AC formulation. Hashemi and Zamzamian [7] presented a new multidimensional characteristic-based scheme (MCB) used in conjunction with the artificial compressibility method which could accurately solve incompressible flows. Zhang *et al.* [8] developed a combined method by spectral collocation (SC) and artificial compressibility method (AC) methods to solve 2D steady flows. Their results show that the new scheme named SCM-ACM has simultaneous advantages of both individual methods like high accuracy, convergence, and efficiency. Zhang *et al.* [9] used the same aforementioned combined method (SCM-ACM) to investigate radiation effects on magneto hydrodynamics (MHD) natural convection. Loppi *et al.* [10] successfully applied the dual-time stepping ACM in conjunction with the flux reconstruction (FR) discretization to obtain a high-order cross-platform incompressible Navier-Stokes solver. A more recent approach is the one proposed by Pranowo and Wijayanta [11] in which a direct meshless local Petrov-Galerkin method was combined with implicit AC to simulate a natural convection problem. Some convergence acceleration techniques are also implemented with ACM which are available in the literature [12].

Another difficulty in numerical simulation of incompressible flows is the nonphysical oscillation usually arises when central differencing is used to discretize convective terms. These oscillations can unfavorably affect the convergence, stability, and accurate results. Fortunately, these fluctuations can be smeared out by adding artificial dissipation (AD) terms into the governing equations. Various artificial dissipation models are available in the literature. Svärd *et al.* [13] introduced first, second, and fourth-order Laplacian-based dissipation operators. Hashimoto *et al.* [14] integrated the solution with a spatial filter which can eliminate grid-to-grid oscillations when using a coarser grid and reduce high-frequency spurious oscillations. Recently, Krimi *et al.* [15] used an automatic adaptive numerical dissipation scheme to solve weakly compressible flows.

Jameson *et al.* [16] introduced an efficient artificial dissipation model which is made up of second and fourth differences of primitive variables with coefficients dependent on local pressure gradients. This method can effectively reduce unwanted wiggles produced in numerical solutions of Euler equations in the wide range of Mach numbers. Singh [17] demonstrated the versatility of the Jameson scheme in hypersonic flows with Mach numbers up to 50 without real gas effects. Hashemi and Jahangirian [18] successfully implemented the Jameson method in hypersonic laminar flows considering real gas effects. Li *et al.* [19] extended this efficient approach to compressible viscous flows. Esfahanian and Akbarzadeh [20] adopted the Jameson method to simulate steady incompressible viscous and inviscid flows in three different problems. Despite efficient operation and being easy to use, the Jameson

method rarely is implemented to solve Navier-Stokes equations, especially in unsteady form. Also, the Jameson method is mostly used in the aerodynamics field in which Euler equations are often considered as governing equations. To the best of the author's knowledge, the Jameson method has not used for solving unsteady Navier-Stokes equations in lid-driven cavity with nanofluid flow. In this paper, a FORTRAN code is developed to numerically simulate unsteady incompressible nanofluid flow in lid-driven cavity using artificial compressibility method in conjunction with Jameson Artificial dissipation scheme. The present method is validated by simulating the flow field in lid-driven cavity at various Reynolds and Grashof numbers. At last, the goal of the present work is to study the capability of the Jameson artificial dissipation scheme to numerically simulate the mixed convection heat transfer in Cu-water nanofluid flow at a different volume fraction of nanoparticles.

2. Governing equations

Unsteady incompressible 2D Navier-Stokes equations, which have mathematically elliptic behavior, are the governing equations of the present problem. According to the artificial compressibility method, the pseudo-time derivative of pressure is added to the continuity equation to couple the velocity and pressure fields and transform the nature of equations into hyperbolic which enables the use of the time marching methods [20].

$$\begin{aligned}
&\frac{1}{\beta^2}\frac{\partial p}{\partial \tau}+\frac{\partial u}{\partial x}+\frac{\partial v}{\partial y}=0\\
&\frac{\partial u}{\partial t}+\frac{\partial}{\partial x}\left(u^2+\frac{p}{\rho_{nf}}\right)+\frac{\partial}{\partial y}(uv)=\nu_{nf}\left(\frac{\partial^2 u}{\partial x^2}+\frac{\partial^2 u}{\partial y^2}\right)\\
&\frac{\partial v}{\partial t}+\frac{\partial}{\partial x}(uv)+\frac{\partial}{\partial y}\left(v^2+\frac{p}{\rho_{nf}}\right)=\nu_{nf}\left(\frac{\partial^2 v}{\partial x^2}+\frac{\partial^2 v}{\partial y^2}\right)+g\zeta_{nf}\Delta T\\
&\frac{\partial T}{\partial t}+\frac{\partial}{\partial x}(uT)+\frac{\partial}{\partial y}(uT)=\alpha_{nf}\nu\left(\frac{\partial^2 T}{\partial x^2}+\frac{\partial^2 T}{\partial y^2}\right),
\end{aligned} \tag{1}$$

where β is the artificial compressibility parameter and considered to be constant and equal to one ($\beta=1$) [20]. Also, τ represents pseudo time, while t denotes the real time.

Various relations are available for thermo physical properties of nanofluids [21] but in this study simple formulations will be adequate. Effective density (ρ_{nf}) and heat capacitance $(\rho C_p)_{nf}$ of nanofluid are obtained as follows [22]:

$$\begin{aligned}
&\rho_{nf}=\rho_f(1-\phi)+\rho_s\phi,\\
&(\rho C_p)_{nf}=(\rho C_p)_f(1-\phi)+(\rho C_p)_s\phi \quad ,
\end{aligned} \tag{2}$$

where ϕ represents the volume fraction of nanoparticles. The dynamic viscosity of nanofluid is determined according to Brinkman's [23] proposal:

$$\mu_{nf}=\frac{\mu_f}{(1-\phi)^{2.5}}\ , \tag{3}$$

Thermal conductivity, which is needed to calculate thermal diffusivity (α_{nf}), is obtained as [24]:

$$\begin{aligned}
&\frac{k_{nf}}{k_f}=\frac{k_s+2k_f-2\phi(k_f-k_s)}{k_s+2k_f+\phi(k_f-k_s)},\\
&\alpha_{nf}=\frac{k_{nf}}{(\rho C_p)_{nf}},
\end{aligned} \tag{4}$$

The thermal expansion coefficient of nanofluid is defined as [24]:

$$\zeta_{nf}=\zeta_f(1-\phi)+\zeta_s\phi \tag{5}$$

The thermophysical properties of the base fluid and the nanoparticles are listed in Table 1.
In unsteady problems, pseudo-time derivatives of velocities and temperature must be added to momentum and energy equations, respectively.

Table 1. Thermophysical properties of water and Cu nanoparticles [24]

	ρ (kg/m^3)	C_p $(J/kg.K)$	K $(w/m,K)$	ζ $(1/K)$
Water	997.1	4179	0.613	21
Copper (Cu)	8933	385	401	1.67

So, the governing equations of two-dimensional unsteady incompressible viscous flow with heat transfer in non-dimensional form are modified as:

$$\begin{aligned}
&\frac{\partial p^*}{\partial \tau^*}+\beta^{*2}\left(\frac{\partial u^*}{\partial x^*}+\frac{\partial v^*}{\partial y^*}\right)=0\\
&\frac{\partial u^*}{\partial \tau^*}+\frac{\partial u^*}{\partial t^*}+\frac{\partial}{\partial x^*}\left(u^{*2}+p^*\right)+\frac{\partial}{\partial y^*}\left(u^*v^*\right)=\frac{1}{\mathrm{Re}}\left(\frac{\partial^2 u^*}{\partial x^{*2}}+\frac{\partial^2 u^*}{\partial y^{*2}}\right)\\
&\frac{\partial v^*}{\partial \tau^*}+\frac{\partial v^*}{\partial t^*}+\frac{\partial}{\partial y^*}\left(v^{*2}+p^*\right)+\frac{\partial}{\partial x^*}\left(u^*v^*\right)=\frac{1}{\mathrm{Re}}\left(\frac{\partial^2 v^*}{\partial x^{*2}}+\frac{\partial^2 v^*}{\partial y^{*2}}\right)+\frac{\mathrm{Gr}}{\mathrm{Re}^2}T^*\\
&\frac{\partial T^*}{\partial \tau^*}+\frac{\partial T^*}{\partial t^*}+\frac{\partial}{\partial x^*}\left(u^*T^*\right)+\frac{\partial}{\partial y^*}\left(u^*T^*\right)=\frac{1}{\mathrm{Re.Pr}}\left(\frac{\partial^2 T^*}{\partial x^{*2}}+\frac{\partial^2 T^*}{\partial y^{*2}}\right),
\end{aligned} \tag{6}$$

where $\mathrm{Re}=\rho_{nf}u_h L/\mu_{nf}$ is the Reynolds number, $Gr=g\zeta_{nf}L^3(T_h-T_c)/\nu_{nf}^2$ is Grashof number, $Pr=\nu_{nf}/\alpha_{nf}$ is Prandtl number in which α_{nf} represents the thermal diffusivity, ζ_{nf} is the thermal expansion coefficient and other variables are obtained as [7]:

$$\begin{aligned}
&x^*=\frac{x}{L},\ y^*=\frac{y}{L},\ u^*=\frac{u}{u_h},\ v^*=\frac{v}{u_h},\ p^*=\frac{p}{\rho_{nf}u_h^2},\\
&\rho^*=\frac{\rho}{\rho_{nf}},\ T^*=\frac{T-T_s}{T_h-T_s},\ t^*=\frac{tu_h}{L},\ \beta^*=\frac{\beta}{u_h}
\end{aligned} \tag{7}$$

Square cavity filled with Cu-water nanofluid is considered as Fig. 1. The vertical walls are insulated and the horizontal walls are in constant temperature. The upper wall with high temperature is moving with uniform velocity along x direction. Buoyancy force besides the movement of the hot wall induces a flow inside the cavity. The following assumptions are made in this simulation:

a. Laminar regime is dominant in the cavity.
b. The flow is viscous and incompressible.
c. Boussinesq approximation is valid for buoyancy force.
d. Both water and copper nanoparticles are in thermal and chemical equilibrium.
e. The solid particles sizes assumed to be nanometric (less than 10 nm) and small enough to behave similar to liquid molecules.
f. The Cu-water nanofluid is considered as a single-phase fluid and assumed that the nanofluid is well prepared.

The system of governing equations can be written in vector form which eases the manipulation of the equation system. The system of Eq. (6) is manipulated to get its vector form, then in the time integration process, pseudo-time derivatives are involved.

$$\frac{\partial \mathbf{W}}{\partial \tau^*}+\frac{\partial \bar{\mathbf{W}}}{\partial t^*}+\frac{\partial \mathbf{F}}{\partial x^*}+\frac{\partial \mathbf{G}}{\partial y^*}=\frac{1}{\mathrm{Re}}\left(\frac{\partial \mathbf{R}}{\partial x^*}+\frac{\partial \mathbf{S}}{\partial y^*}\right)+\mathrm{Ri}\times\mathbf{H} \tag{8}$$

where, **W** is the unknown primitive conservative variables, F and G are convective fluxes in the x and y directions, R and S are viscous fluxes in x and y directions, respectively, and $Ri=Gr/Re^2$ denotes Richardson number. These vectors contain the following variables:

$$\begin{aligned}
&\mathbf{W}=\begin{bmatrix}p^*\\u^*\\v^*\\T^*\end{bmatrix},\ \bar{\mathbf{W}}=\begin{bmatrix}0\\u^*\\v^*\\T^*\end{bmatrix},\ \mathbf{F}=\begin{bmatrix}\beta u^*\\u^{*2}+p^*\\u^*v^*\\u^*T^*\end{bmatrix},\ \mathbf{G}=\begin{bmatrix}\beta v^*\\u^*v^*\\v^{*2}+p^*\\v^*T^*\end{bmatrix},\\
&\mathbf{R}=\begin{bmatrix}0\\\frac{\partial u^*}{\partial x^*}\\\frac{\partial v^*}{\partial x^*}\\\frac{1}{\mathrm{Pr}}\frac{\partial T^*}{\partial x}\end{bmatrix},\ \mathbf{S}=\begin{bmatrix}0\\\frac{\partial u^*}{\partial y^*}\\\frac{\partial v^*}{\partial y^*}\\\frac{1}{\mathrm{Pr}}\frac{\partial T^*}{\partial y^*}\end{bmatrix},\ \mathbf{H}=\begin{bmatrix}0\\0\\T^*\\0\end{bmatrix}
\end{aligned} \tag{9}$$

3. Finite volume numerical implementation

Cell-centered finite volume approach is implemented to approximate spatial derivatives. Both viscous and convective terms are discretized with a second-order central scheme.

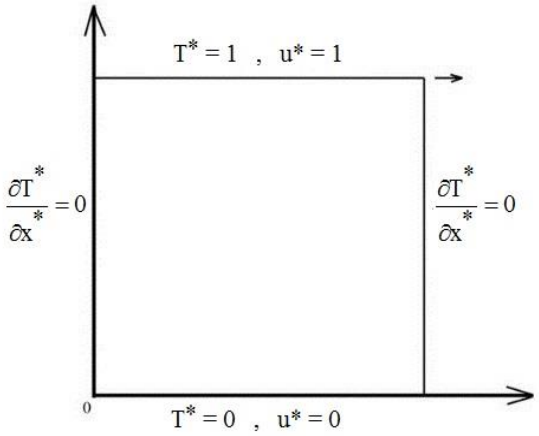

Fig. 1. Geometry and boundary condition.

So, integrating from Eq. (8) in real time over volumes of cells and using the Green hypothesis on integrals of fluxes gives:

$$\frac{\partial}{\partial t}\iint_s \bar{\mathbf{W}}dx^*dy^* + \oint_c (\mathbf{F}dy^* - \mathbf{G}dx^*) = \frac{1}{\mathrm{Re}}\oint_c (\mathbf{R}dy^* - \mathbf{S}dx^*) + \mathrm{Ri}\iint_s \mathbf{H}dxdy \quad (10)$$

W and **H** is assumed invariant inside cells, and then Eq. (10) can be further simplified:

$$\frac{\partial(\bar{\mathbf{W}}A)_i}{\partial t^*} + \mathbf{Q}_i(\mathbf{W}) = 0$$
$$\mathbf{Q}_i(\mathbf{W}) = \sum_{k=1}^{n}\left[\left(\mathbf{F} - \frac{1}{\mathrm{Re}}\mathbf{R}\right)\Delta y^* - \left(\mathbf{G} - \frac{1}{\mathrm{Re}}\mathbf{S}\right)\Delta x^*\right]_k - \frac{\mathrm{Gr}}{\mathrm{Re}^2}\mathbf{H}_i A_i = 0 \quad (11)$$

Central schemes in convective terms produce nonphysical oscillations in numerical procedure. Jameson added an artificial dissipation term ($\mathbf{D}_i(\mathbf{W})$) to Eq. (11) to overcome this problem. This term is the combination of second and fourth differences of primitive variables [25]. The first part is to eliminate wiggles around discontinuities like shockwaves and the later one to suppress the oscillations inside the domain:

$$\frac{\partial(\bar{\mathbf{W}}A)_i}{\partial t^*} + \mathbf{Q}_i(\mathbf{W}) - \mathbf{D}_i(\mathbf{W}) = 0, \mathbf{D}_i(\mathbf{W}) = \sum_{k=1}^{n}\mathbf{d}_k^{(2)} + \sum_{k=1}^{n}\mathbf{d}_k^{(4)}$$
$$\mathbf{d}_k^{(2)} = \lambda_k \varepsilon_k^{(2)}(\mathbf{W}_L - \mathbf{W}_R)_k \quad , \quad \mathbf{d}_k^{(4)} = \lambda_k \varepsilon_k^{(2)}(\Delta^2\mathbf{W}_L - \Delta^2\mathbf{W}_R)_k \quad (12)$$
$$\Delta^2\mathbf{W}_i = \sum_{k=1}^{n}(\mathbf{W}_L - \mathbf{W}_R)_k$$

In the last two relations, $\mathbf{d}_k^{(2)}$ and $\mathbf{d}_k^{(4)}$ indicates the dissipation terms based on the second and fourth differences of **W**, respectively; and λ_k is calculated according to a maximum value of the Jacobin matric of $\partial\mathbf{F}/\partial\mathbf{W}$ and $\partial\mathbf{G}/\partial\mathbf{W}$ as below [25, 26]:

$$\lambda_k = \left|\bar{u}_k^*\Delta y_k - \bar{v}_k^*\Delta x_k\right| + \bar{c}\sqrt{\Delta x_k^{*2} + \Delta y_k^{*2}}\,,$$
$$\bar{c} = \sqrt{\vec{V}_k^*.\vec{n}_k + \beta} \quad , \vec{V}_k^* = \bar{u}_k^*\vec{i} + \bar{v}_k^*\vec{j} \quad (13)$$

where $\bar{u}^*$ and $\bar{v}^*$ are average non-dimensional velocity components on the face k and $\vec{n}_k$ is the normal unit vector of face k.

Dual-time stepping approach is used to discretize temporal terms. To discretize unsteady terms, second order implicit method which has a better stability is utilized;

$$\frac{3\bar{\mathbf{W}}_i^{n+1}A_i^{n+1} - 4\bar{\mathbf{W}}_i^{n}A_i^{n} - \bar{\mathbf{W}}_i^{n-1}A_i^{n-1}}{2\Delta t_i^*} + \mathbf{Qn}_i(\mathbf{W}^{n+1}) = \hat{\mathbf{Q}}_i(\mathbf{W}) \quad (14)$$
$$\mathbf{Qn}_i(\mathbf{W}) = \mathbf{Q}_i(\mathbf{W}) - \mathbf{D}_i(\mathbf{W})$$

Here, n is the real time step. In unsteady problems, adding pseudo-time derivatives of conservative variables to Eq. (1) enables marching in nonphysical time (τ^*). Therefore, each real time step is divided into several inner time steps and convergence in this pseudo-time results in convergence of current real time step which occurs when $\hat{\mathbf{Q}}_i(\mathbf{W})$ tends to 0. So, the:

$$A_i\frac{\partial \boldsymbol{W}^{n+1}{}_i}{\partial \tau^*} + \hat{\boldsymbol{Q}}_i(\boldsymbol{W}^{n+1}) = 0 \quad (15)$$

First order explicit discretization is implemented to approximate this ODE and then is solved by fourth order Runge-Kutta method [27].

The stop criterion in pseudo-time is pressure differences as:

$$Res = log\left(\sum_{i=1}^{N}\left|\frac{P_i^{*n} - P_i^{*n+1}}{\Delta\tau_i^*}\right|\right) \quad (16)$$

To accelerate the convergence rate, residual smoothing technique is implemented in pseudo-time steps [27].

The local Nusselt number (Nu_L) and average Nusselt number ($\overline{Nu}$) along an isothermal wall are defined as [24]:

$$Nu_L = \frac{k_{nf}}{k_f}\left[\frac{\partial T^*}{\partial y^*}\right]_{y=1} \quad , \quad \overline{Nu} = \int_0^1 \frac{k_{nf}}{k_f}\left[\frac{\partial T^*}{\partial y^*}\right]_{y^*=1} dx^* \quad (17)$$

4. Results and discussion

4.1. Grid study and developed code validation

In this paper unstructured grid is used to discretize the domain. This type of mesh is popular in literature due to its compatibility with complex geometries. A sample of the generated triangular grid has been shown in Fig. 2.

To study the independence of results from the size of the generated grid, five different grid cases and the number of cells are evaluated in Table 2.

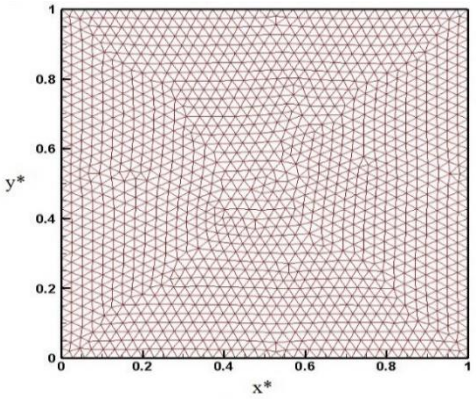

Fig. 2. Unstructured grid of the cavity with triangular elements

Table 2. Five different meshes used to study the grid independence

	Number of cells	Number of nodes on walls	Number of nodes on each wall
Case 1	2030	120	30
Case 2	4550	180	45
Case 3	7988	240	60
Case 4	14404	320	80
Case 5	22512	400	100

Variation of x^*-direction velocity (u^*) along the central horizontal line (y^*=0.5) of the cavity for each case of meshes in Re=3000 is plotted in Fig. 3. It is shown that there is a small difference between cases, but this negligible difference becomes greater in lower half of the cavity. To distinguish these differences and choose the best grid, a magnified view is plotted as well. Results show a matching values for cases 4 and 5. Then, case 4 is selected for next simulations. Validation is performed according to the results of Ghia *et al.* [28] and Iwatsu *et al.* [29]. In Fig. 4, the velocity components on the central lines of the cavity are compared with Ghia et al's research in which laminar flow without heat transfer is investigated. In Fig. 5, the local Nusselt number along hot wall is compered between the present study and that of Iwatsu *et al.* [29] for Re=400 at two Grashf numbers and average Nusselt number on the hot wall for both $Gr=10^2$,10^6 and Re=400,1000 in Table 3. All comparisons show a good agreement between the results of the current study and the literature. Besides of accuracy, the convergence rate is an important parameter of a scheme. Then, the convergence history of the Jameson's method, which is accelerated with residual smoothing technique, is illustrated in Fig. 6 under Reynolds number of 1000 and Grashof number of 10^6.

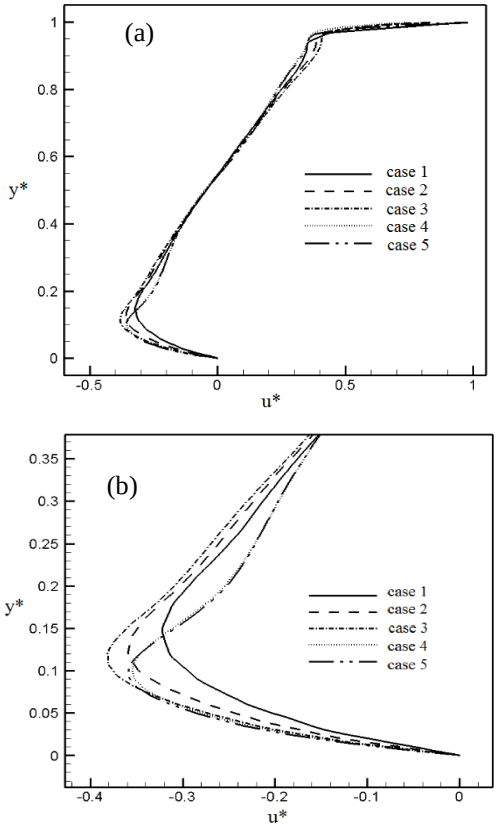

Fig. 3. (a) u^*-y^* diagram of different cases for Re=3000 and (b) close view of velocity distribution with most difference in results of meshes.

4.2. Effects of parameters

The influence of Grashof number ($Gr=10^2$, 10^6) and volume fraction of nanoparticles (ϕ=0, 0.03, 0.05) is investigated in this paper. Low volume fraction values are chosen to ensure the stability of nanofluid and uniform distribution of nanoparticles. The obtained results show no significant difference between streamlines of different volume fractions at $Gr=10^2$ while temperature contours show a slight expand for the hot core with a drop in the central parts of the cavity by increasing volume fraction. When $Gr=10^6$, natural convection becomes more significant and a mixed convection is dominant in the cavity.

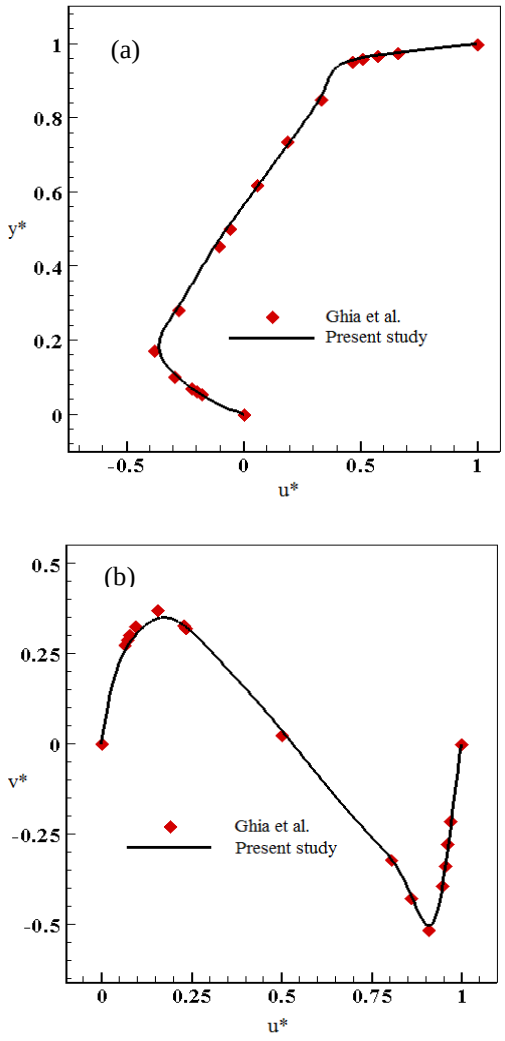

Fig. 4. Comparison of velocity components of the present study and Ghia *et al.* [28] Re=1000 (a) u^*-y^* (b) x^*-v^*

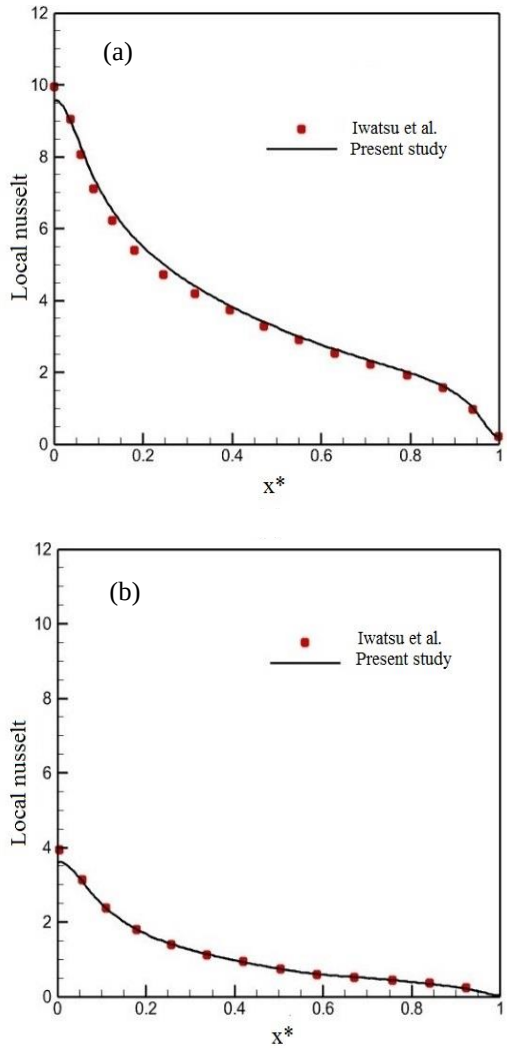

Fig. 5. Comparison of local Nusselt number along the hot wall between the present study and Iwatsu *et al.* [29] for Re=400 (a) $Gr=10^2$ and (b) $Gr=10^6$.

Figs. 7 and 8 indicate the streamlines and temperature contours respectively, under Re=1000 and $Gr=10^6$ for three mentioned volume fractions. In Fig. 7, it is obvious that when the working fluid is pure (ϕ=0) three main vortexes have filled the whole width of the cavity. By increasing volume fraction, the upper vortex tends to overcome to the lower vortexes and the central vortex is more stretched. Eventually, when ϕ=0.05, two lower vortexes join to each other while the upper one gets stronger and tends to take apart the lower vortex into the left and right corner vortexes which is observed in forced convection in Fig. 7.

Table 3. Comparison of average Nusselt number on the hot wall.

	$Gr = 10^2$		$Gr = 10^6$	
Re	Iwatsu *et al.* [29]	present study	Iwatsu *et al.* [29]	present study
400	3.84	3.78	1.22	1.19
1000	6.33	6.22	1.77	1.68

It is shown from temperature contours that when ϕt (Fig. 8(a)), a hot part with a high-temperature core has filled almost half of the cavity. The middle area has a medium temperature and the lowest part is cold. The hot section is wavy while two other sections are laminar.

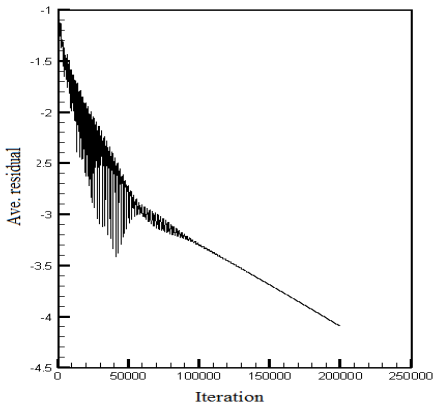

Fig. 6. Convergence history at Gr=10^6 for Re=1000.

By increasing the volume fraction, the hot core gets stronger and expands pushing the colder layers into the bottom of the cavity. In other words, as ϕ increases, hot nanofluid is diffused in more regions of the cavity.

By comparing two temperature contours at the same ϕ in two different Grashof numbers, it can be concluded that a decrease in Gr number improves heat distribution due to the domination of forced convection.

Fig. 9 shows the non-dimensional y-direction velocity (v^*) on the horizontal central line of the cavity (y^*=0.5) under both Gr=10^2 and Gr=10^6 for three volume fractions. Fig. 10 shows the non-dimensional x-direction velocity (u^*) on the vertical central line of the cavity (x^*=0.5) at Gr=10^6 for three volume fractions.

The results show that there is no considerable difference between the diagrams of various volume fractions at Gr=10^2, while notable augmentation is seen at Gr=10^6 as ϕ increases. For pure water, only the fluid of the upper half of the cavity is influenced by the moving wall and the rest of the fluid is motionless. But more regions of the cavity are affected by the motion of the hot wall and a significant augmentation in velocity values is obvious as ϕ increases.

Both u* and v* have a similar behavior in different Gr numbers. That means when Gr=10^2, variation of ϕ has no meaningful effect on velocity diagrams; but in contrast, changes in the motion area and velocity magnitudes are considerable. This jump in velocity magnitudes causes better fluid circulation inside the cavity which helps heat distribution, confirming the results concluded from Fig. 8.

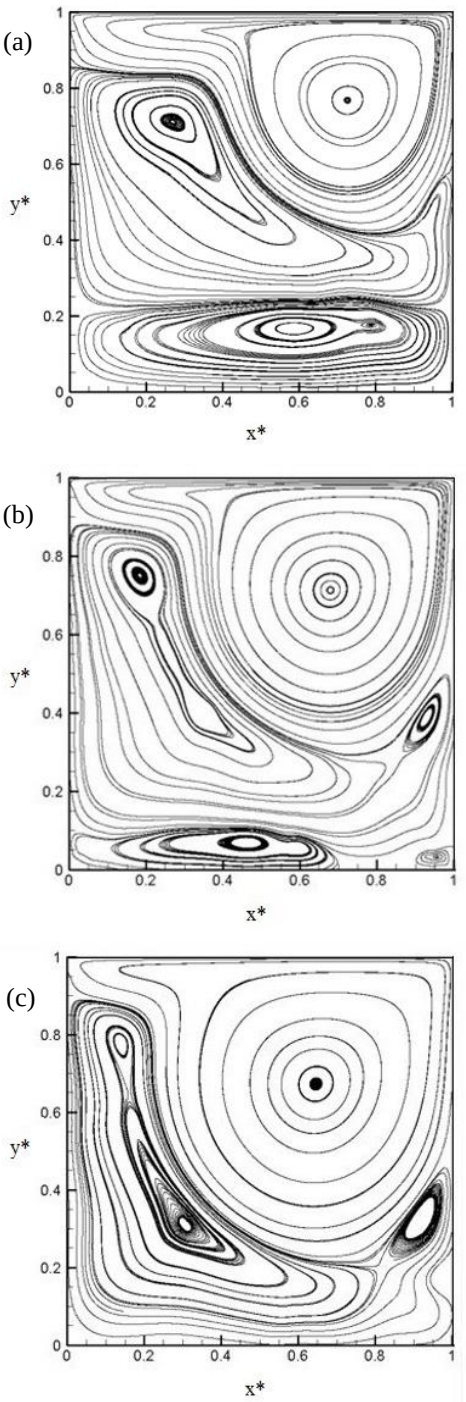

Fig. 7. Comparison of streamlines at Re=1000 and Gr=10^6 for a) ϕ=0 b) ϕ=0.03 c) ϕ=0.05.

Fig. 11 shows the average Nusselt number along the hot wall for both Gr numbers. For both Gr numbers, an increase in volume fraction enhances the average Nusselt number which is the main effect of nanoparticles in comparison with pure water.

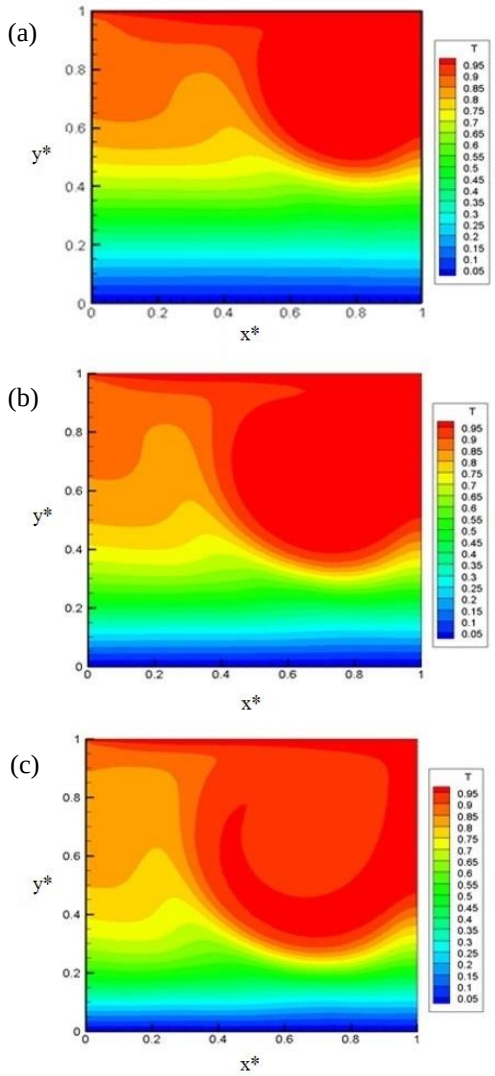

Fig. 8. Comparison of temperature contours at Re=1000 and Gr=10^6 for a) ϕ=0 b) ϕ=0.03 c) ϕ=0.05.

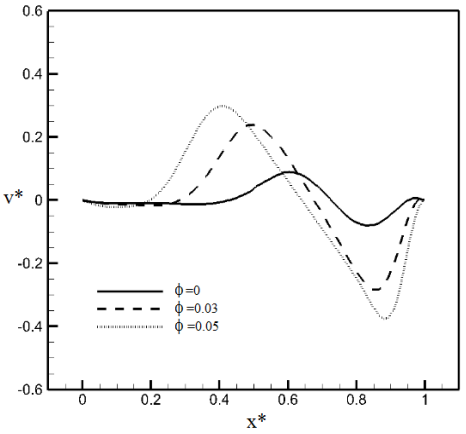

Fig. 9. Comparison of x^*-v^* diagrams for Gr=10^6 at Re=1000 and ϕ=0, 0.03, 0.05.

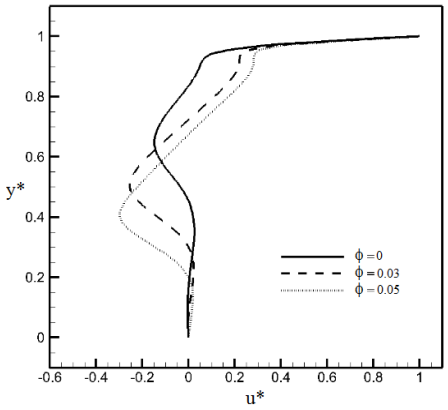

Fig. 10. Comparison of u^*-y^* diagrams for Gr=10^6 at Re=1000 and ϕ=0, 0.03, 0.05.

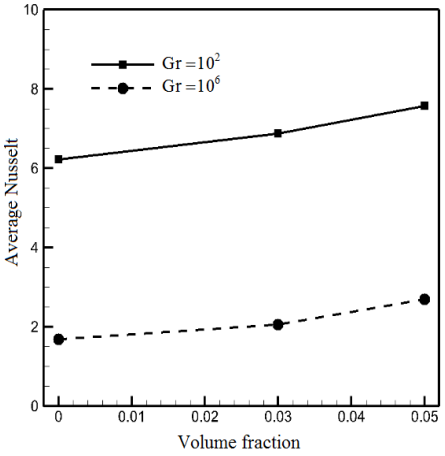

Fig. 11. Comparison of average Nusselt number along the hot wall for Gr=10^2 and Gr=10^6 under Re=1000 at different volume fractions of nanoparticles

5. Conclusions

A FORTRAN code is developed to simulate an unsteady and viscous nanofluid flow in a lid-driven cavity by implementing the Jameson method coupled with the artificial compressibility method. This combination of numerical methods has not been used in an unsteady and nanofluid flow to the best knowledge of the authors. It is found that the Jameson method has good performance with a reasonable convergence rate. The obtained results for pure water show a good agreement between the results of the current study and the literature. Effects of Grashof number and nanoparticle volume fraction on the flow and heat transfer characteristics are investigated.

Also, the observations made from this investigation are listed as follows:

(i) An increase in volume fraction of nanoparticles improves heat transfer characteristics.
(ii) The velocity of Cu-water nanofluid increases with the enhanced nanoparticle volume fraction.
(iii) An increase in volume fraction of nanoparticles improves average Nusselt number while increment of Gr number reduces the Nusselt number.
(iv) A 52% and 16% growth in average Nusselt number can be gained by an increase in VF from 0 to 0.05 in $Gr=10^2$ and $Gr=10^6$ respectively.

References

[1] A. J. Chorin, "A Numerical Method for Solving Incompressible Viscous Flow Problems", *J. Comput. Phys.* Vol. 2, No. 1, pp. 12-26, (1967).

[2] A. G. Malan, R. W. Lewis and P. Nithiarasu, "An improved unsteady, unstructured, artificial compressibility, finite volume scheme for viscous incompressible fows: Part I. Theory and implementation", *Int. J. Numer. Methods. Eng.*, Vol. 54, No. 5 pp. 695-714, (2002).

[3] A. G. Malan, R. W. Lewis and P. Nithiarasu, "An improved unsteady, unstructured, artificial compressibility,finite volume scheme for viscous incompressible fows: PartII. application", *Int. J. Numer. Methods Eng.*, Vol. 54, No. 5, pp. 715-729, (2002).

[4] P. Louda, K. Kozel and J. Prihoda, "Numerical solution of 2D and 3D viscous incompressible steady and unsteady flows using artificial compressibility method", *Int. J. Numer. Methods. Fluids*, Vol. 56, No. 8, pp. 1399-1407, (2008).

[5] C. Liang, A. S. Chan and A. Jameson, "A p-multigrid spectral difference method for two-dimensional unsteady incompressible Navier–Stokes equations", *Comput. Fluids*, Vol. 51, No. 1, pp. 127-135, (2011).

[6] H. S. Tang and F. Sotiropoulos, "Fractional step artificial compressibility schemes for the unsteady incompressible Navier–Stokes equations", *Comput. Fluids*, Vol. 36, No. 5, pp. 974-986, (2007).

[7] M. Y. Hashemi and K. Zamzamian, "A multidimensional characteristic-based method for making incompressible flow calculations on unstructured grids", *J. Comput. Appl. Math.*, Vol. 259, Part B, pp. 752-759, (2014).

[8] J. Zhang, H. Dong, E. Zhou, B. Li and X. Tian, "A combined method for solving 2D incompressible flow and heat transfer by spectral collocation method and artificial compressibility method", *Int. J. Heat Mass Transf.*, Vol. 112, pp. 289-299, (2017).

[9] J. Zhang, B. Li, H. Dong, X. Luo and H. Lin, "Analysis of magnetohydrodynamics (MHD) natural convection in 2D cavity and 3D cavity with thermal radiation effects", *Int. J. Heat Mass Transf.*, Vol. 112, pp. 216-223, (2017).

[10] N. A. Loppi, F. D. Witherden, A. Jameson and P. E. Vincent, "A high-order cross-platform incompressible Navier–Stokes solver via artificial compressibility with application to a turbulent jet", *Comput. Phys. Commun.*, Vol. 223, pp. 193-205, (2018).

[11] A. Pranowo and A. T. Wijayanta, "Numerical solution strategy for natural convection problems in a triangular cavity using a direct meshless local Petrov-Galerkin method combined with an implicit artificial-compressibility model", *Eng. Anal. Boundary Elem.*, Vol. 126, pp. 13-29, (2021).

[12] N. A. Loppi, F. D. Witherden, A. Jameson and P. E. Vincent, "Locally adaptive pseudo-time stepping for high-order flux reconstruction," J. Comput. Phys., Vol. 399, No. 6, p.108913, (2019).

[13] M. Svärd, J. Gong and J. Nordström, "Stable artificial dissipation operators for finite volume schemes on unstructured grids", *Appl. Numer. Math.*, Vol. 56, No. 12, pp. 1481-1490, (2006).

[14] T. Hashimoto, I. Tanno, T. Yasuda, Y. Tanaka, K. Morinishi and N. Satofuka, "Optimized finite difference method with artifcial dissipation for under-resolved

unsteady incompressible flow computations using kinetically reduced local Navier-Stokes equations", *Comput. Fluid*, Vol. 184, pp. 21-28, (2019).

[15] A. Krimi, L. Ramírez, S. Khelladi, F. Navarrina, M. Deligant and X. Nogueira, "Improved δ-SPH Scheme with Automatic and Adaptive Numerical Dissipation", *Water*, Vo. 12, No. 10, pp. 1-24, (2020).

[16] A. Jameson, W. Schmit and E. Turkel, "Numerical solutions of the Euler equations by finite volume methods using Runge-Kutta time-stepping schemes", *AlAA 14th Fluid and Plasma Dynamics Conference*, Palo Alto, California, June 23-25, (1981).

[17] J. P. Singh, "Evaluation of Jameson-Schmit-Turkel dissipation scheme for hypersonic flow computations", *J. Aircr*, Vol. 33, No. 2, pp. 286-290, (1996).

[18] M. Y. Hashemi and A. Jahangirian, "Simulation of high-speed flows by an unstructured grid implicit method including real gas effects", *Int. J. Numer. Meth. Fluids*, Vol. 56, No. 8, pp. 1281-1287, (2008).

[19] J. Li, F. Li and E. Qin, "A fully implicit method for steady and unsteady viscous flow simulations", *Int. J. Numer. Meth. Fluids*, Vol. 43, No. 2, pp. 147-163, (2003).

[20] V. Esfahanian and P. Akbarzadeh, "The Jameson's numerical method for solving the incompressible viscous and inviscid flows by means of artificial compressibility and preconditioning method", *Appl. Math. Comput.*, Vol. 206, No. 2, pp. 651-661, (2008).

[21] B. Bakthavatchalam, K. Habib, R. Saidur, B. B. Saha and K. Irshad, "Comprehensive study on nanofluid and ionanofluid for heat transfer enhancement: A review on current and future perspective", *J. Mol. Liq.*, Vol. 305, p. 112787, (2020).

[22] M. E. Nakhchi and J. A. Esfahani, "Numerical investigation of turbulent Cu-water nanofluid in heat exchanger tube equipped with perforated conical rings", *Adv. Powder Technol.*, Vol. 30, No. 7, pp. 1338-1347, (2019).

[23] H. C. Brinkman, "The Viscosity of Concentrated Suspensions and Solutions", *J. Chem. Phys.*, Vol. 20, No. 4, p. 571, (1952).

[24] S. Soleimani, M. Sheikholeslami, D. D. Ganji and M. Gorji-Bandpay, "Natural convection heat transfer in a nanofluid filled semi-annulus enclosure", *Int. Commun. Heat Mass Transfer*, Vol. 39, No. 4, pp. 565-574, (2012).

[25] A. Jahangirian and M. Y. Hashemi, "Adaptive Cartesian grid with mesh-less zones for compressible flow calculations", *Comput. Fluids*, Vol. 54, pp. 10-17, (2012).

[26] K. Zamzamian and M. Y. Hashemi, "A novel meshless method for incompressible flow calculations", *Eng. Anal. Boundary Elem.*,Vol. 56, pp. 106-118, (2015).

[27] M. Y. Hashemi and A. Jahangirian, "An efficient implicit mesh-less method for compressible flow calculations", *Int. J. Numer. Meth. Fluids*, Vol. 67, No. 6, pp. 754-770, (2011).

[28] U. Ghia, K. N. Ghia and C. T. Shin, "High-resolutions for incompressible flow using the Navier-Stokes equations and a multigrid method", *J. Comput. Phys.*, Vol. 48, No. 3, pp. 387-411,(1982).

[29] R. Iwatsu, J. M. Hyuv and K. Kuwahara, "Mixed convection in a driven cavity with a stable vertical temperature gradient penalty function and artificial compressibility", *Int. J. Heat Mass Transfer*, Vol. 36, No. 6, pp. 1601-1608, (1993).

How to cite this paper:

S. Rasoolzadeh and M.Y. Hashemi, "Numerical solution of unsteady incompressible nanofluid flow with mixed convection heat transfer using Jameson method on unstructured grid,", *J. Comput. Appl. Res. Mech. Eng.*, Vol. 13, No. 2, pp. 169-180, (2024).

DOI: 10.22061/JCARME.2023.9030.2221

URL: https://jcarme.sru.ac.ir/?_action=showPDF&article=1974